

Competitive Multi-Operator Reinforcement Learning for Joint Pricing and Fleet Rebalancing in AMoD Systems

Emil Kragh Toft¹, Carolin Schmidt², Daniele Gammelli³, Filipe Rodrigues¹

Abstract—Autonomous Mobility-on-Demand (AMoD) systems promise to revolutionize urban transportation by providing affordable on-demand services to meet growing travel demand. However, realistic AMoD markets will be competitive, with multiple operators competing for passengers through strategic pricing and fleet deployment. While reinforcement learning has shown promise in optimizing single-operator AMoD control, existing work fails to capture competitive market dynamics. We investigate the impact of competition on policy learning by introducing a multi-operator reinforcement learning framework where two operators simultaneously learn pricing and fleet rebalancing policies. By integrating discrete choice theory, we enable passenger allocation and demand competition to emerge endogenously from utility-maximizing decisions. Experiments using real-world data from multiple cities demonstrate that competition fundamentally alters learned behaviors, leading to lower prices and distinct fleet positioning patterns compared to monopolistic settings. Notably, we demonstrate that learning-based approaches are robust to the additional stochasticity of competition, with competitive agents successfully converging to effective policies while accounting for partially unobserved competitor strategies.

I. INTRODUCTION

Urban mobility systems face growing pressure from rapid urbanization, and evolving consumer expectations. The gap between private vehicle ownership and inflexible public transit has fueled the rapid growth of ride-hailing services, fundamentally transforming urban mobility [1]. Autonomous Mobility-on-Demand (AMoD) systems promise to further revolutionize transportation by enabling affordable door-to-door service at scale [2]. However, unlike regulated public transit monopolies, AMoD markets are likely to be competitive, with multiple operators deploying fleets and competing for passengers.

In such markets, operators must strategically set prices and position their fleet while anticipating competitor actions, e.g., a price reduction by one operator diverts passengers from others. These interactions create a complex, competitive environment where optimal policies depend on competitor behavior.

Reinforcement Learning (RL) has emerged as a powerful approach for AMoD control to derive scalable, near-optimal policies from data without requiring explicit models of demand or competitor strategies. However, existing RL research predominantly addresses centralized, single-operator settings on vehicle rebalancing [3], [4], pricing [5], [6], or both [7], while realistic AMoD systems will be deployed in a competitive context.

This work investigates the impact of competition on policy learning by developing a competitive multi-operator RL framework for joint pricing and fleet rebalancing. We model two operators that simultaneously learn and adapt strategies while competing for passenger demand, which is allocated via a choice model sensitive to prices, travel times, and wages. The main contributions are:

- We formulate a competitive, dual-operator AMoD control problem in which two independent operators jointly learn pricing and rebalancing policies, extending joint control RL from monopolistic to competitive markets.
- We integrate a passenger choice mechanism with wage-dependent price sensitivity into the learning loop, allowing demand allocation between operators to emerge endogenously from their actions.
- Using real-world taxi-trip data from multiple cities, we empirically demonstrate that simultaneous learning in a competitive setting converges, and analyze how competition alters learned strategies, service quality, and market efficiency relative to monopolistic control.

II. LITERATURE REVIEW

Early work on AMoD systems relied on queueing-theoretic models [8] and Model Predictive Control for fleet rebalancing [9], later extended with robust optimization to handle demand uncertainty [10]. While theoretically grounded, these approaches struggle when demand deviates from assumed distributions or computational budgets are exceeded [11]. More recently, RL has emerged as a data-driven alternative, learning policies directly through interaction without explicit demand or traffic models [4]. Gammelli et al. [3] proposed a hierarchical framework for rebalancing that combines the strengths of traditional optimization and RL, using graph neural networks to exploit the spatial structure of transportation networks. By leveraging these tools, RL scales efficiently to large-scale, real-world urban mobility scenarios [12].

While these methods focus on supply, dynamic pricing complements rebalancing by shaping demand. Early pricing work adopted equilibrium-based [13] and operations-research formulations [14], while bi-level models [15] jointly optimize operator and passenger decisions. However, addressing pricing or rebalancing in isolation fails to exploit their synergies [7]. In particular, a recent RL-based framework for joint rebalancing and pricing has shown that joint control consistently outperforms separate strategies [7].

Multi-operator competition has been studied through game-theoretic pricing models [16], agent-based simulation [17], and quality-of-service competition frameworks [18]. However,

¹Technical University of Denmark, Denmark
s233791@student.dtu.dk, rodr@dtu.dk

²Technical University of Munich, Germany
carolin.schmidt@tum.de

³Stanford University, USA gammelli@stanford.edu

these works rely on analytical equilibrium or static models and address either pricing or fleet management in isolation. While reinforcement learning has been explored in single-operator AMoD contexts, this work addresses the competitive multi-operator setting to jointly learn competitive rebalancing and pricing policies with endogenous, price-responsive demand. Specifically, by formulating a dual-operator RL framework where competing operators simultaneously learn policies while competing for demand, this work fills the gap and studies the impact of competition on RL-based policy learning.

III. DESIGN AND IMPLEMENTATION

We represent the AMoD environment as a directed graph $\mathcal{G} = (\mathcal{V}, \mathcal{E})$, where \mathcal{V} comprises N_v spatial regions, each centered on a designated pickup/drop-off station. The total fleet is partitioned between two independent operators controlling M_0 and M_1 autonomous vehicles, respectively. Although we focus on the dual-operator case for clarity, the framework extends trivially to more operators. Both operators act within a synchronized discrete time horizon $\mathcal{T} = \{1, \dots, T\}$ with time steps of 3 minutes. Movement from region i to j follows the shortest path, requiring $\tau_{ij} \in \mathbb{Z}_+$ time steps and incurring a time-variant operational cost c_{ij}^t .

Available supply at station i at time t is characterized by the idle-vehicle counts $m_{i,0}^t$ and $m_{i,1}^t$ of each fleet. On the demand side, passengers arriving at origin i evaluate both AMoD operators and an alternative transportation mode via a discrete choice model: a utility U is computed for each option as a function of trip price, passenger salary, and estimated travel time, mapped to choice probabilities, and sampled from a categorical distribution. Upon selecting an operator, passengers enter a first-come, first-served (FCFS) queue. A maximum waiting threshold of 6 minutes is imposed; if no vehicle is dispatched within this window, the passenger exits the system.

Building on this structure, the following sections formalize the operator interaction. We first cast the pricing and rebalancing task as a Markov Decision Process (MDP), then detail a graph neural network architecture designed to capture the spatial dependencies inherent in dual-operator learning.

A. Competitive AMoD Control

We study a dual-operator AMoD setting in which two independent operators each seek to maximize their own profit within a shared environment. The control architecture follows the hierarchical formulation of [3], [7], enabling scalability to real-world urban scenarios [12]. We adapt this framework to a competitive setting, as a means to study the impact of competition on RL-based policy learning. In practice, the control architecture introduces three steps, illustrated in the appendix. Specifically, at each time step t , the simulation proceeds in three steps: **(1) Pricing & rebalancing:** each operator's policy produces origin-based price scalars and a desired idle-vehicle distribution, where price scalars are then converted to fares by multiplication with OD-base prices estimated from historical data. **(2) Demand assignment:** the stochastic choice model generates passenger requests and assigns them to operators

via the price-dependent choice model. Assigned passengers queue at their departure region and await service in FCFS order, subject to a system-wide maximum waiting time. **(3) Rebalancing execution:** each operator's desired distribution is mapped to rebalancing actions by solving a minimal-cost flow problem (see appendix). Flows are executed independently per operator, vehicle states and queues are updated, and the system transitions to $t+1$, returning the new state and rewards.

B. The AMoD Control Problem as an MDP

We formulate multi-operator AMoD control as an MDP with components $(\mathcal{S}, \mathcal{A}, \mathcal{P}, \mathcal{R})$ defined below.

State space (\mathcal{S}): The state $s_{t,o}$ of operator o at time $t \in \mathcal{T}$ comprises: the network adjacency matrix \mathbf{A} , own idle vehicles per region i as $m_{i,o}^t \in [0, M_o]$, vehicles en route over a planning horizon H_p , $\{m_{i,o}^{t'}\}_{t'=\tau, \dots, \tau+H_p}$, own and competitor prices from last time step $p_{i,j,o}^{t-1}, p_{i,j,o'}^{t-1}$ for all $i, j \in \mathcal{V}$, $o' \neq o$, and own queue lengths $q_{i,o}^t$ and own demand for last time step $d_{i,o}^{t-1}$ for all $i \in \mathcal{V}$. Operators do not share demand or vehicle-location data, but can observe the competitor's prices.

Action space (\mathcal{A}): Each operator o outputs, origin-based price scalars $\rho_{i,o}^t \in (0, 1]$ and a desired idle-vehicle distribution $w_{i,o}^t \in [0, 1]$ with $\sum_{i=1}^{N_v} w_{i,o}^t = 1$, with the latter being used to solve a minimum-cost rebalancing problem. Origin-based price scalars are chosen based on prior work [7], which shows faster convergence and comparable performance to OD-based price scalars. The joint action is $\mathbf{a}_{t,o} = [\mathbf{w}_{t,o}, \rho_{t,o}]$ with $\mathbf{w}_{t,o} = [w_{1,o}^t, \dots, w_{N_v,o}^t]$ and $\rho_{t,o} = [\rho_{1,o}^t, \dots, \rho_{N_v,o}^t]$. The OD fare then calculated as follows:

$$p_{i,j,o}^t = \beta \cdot \rho_{i,o}^t \cdot \bar{p}_{i,j}^t, \quad (1)$$

where $\bar{p}_{i,j}^t$ is a historical reference price (derived from data) and β upper-bounds the price level (we set $\beta = 2$ in our experiments, giving $p_{i,j,o}^t \in (0, 2\bar{p}_{i,j}^t]$).

Reward (\mathcal{R}): Each operator maximizes its own profit, defined as trip revenue minus operational costs:

$$r_o = \sum_{i,j \in \mathcal{V}} x_{i,j,o}^t (p_{i,j,o}^t - c_{i,j,o}^t) - \sum_{(i,j) \in \mathcal{E}} y_{i,j,o}^t c_{i,j,o}^t, \quad (2)$$

where $x_{i,j,o}^t$ denotes passengers served, $y_{i,j,o}^t$ vehicles rebalanced, and $c_{i,j,o}^t$ the per-vehicle travel cost from i to j .

Dynamics (\mathcal{P}): State transitions are driven by stochastic demand, queue updates, and vehicle-availability conservation. The adjacency matrix \mathbf{A} is exogenous and static.

Demand Generation and Mode Choice: The choices of each passenger k are sampled between operator 0, operator 1, or an alternative option (\emptyset) via a Multinomial Logit model with utility

$$U_{k,i,j,o}^t = \beta_0 - \beta_t \cdot v_k \cdot \tau_{i,j}^t - \frac{\bar{v}}{v_k} p_{i,j,o}^t, \quad (3)$$

where β_0 is a baseline preference, β_t the marginal disutility of travel time (set to 0.71, reflecting a 29% undervaluation of time relative to monetary cost, consistent with [19]), v_k the passenger's hourly wage, and \bar{v} the scenario-wide average wage. The ratio \bar{v}/v_k captures income effects. The alternative-option utility is normalized to zero. For each OD-pair (i, j)

and time t , a reference demand $\bar{d}_{i,j}^t$ and price $\bar{p}_{i,j}^t$ are sampled from historical data [20], [21]. The potential demand pool is scaled to $2\bar{d}_{i,j}^t$, and β_0 calibrated such that the total operator demand at historic fare prices is equal the reference demand. The choice model sensitivity to price scalars is shown in the appendix. Wage data are derived from US Census Bureau income statistics [22], with wages for the San Francisco scenario being adjusted using the national US inflation rate from 2008 to 2011 to obtain 2008-equivalent estimates from 2011 data.

Queue and Vehicle Dynamics: The queue for operator o in region i evolves as

$$q_{i,o}^t = q_{i,o}^{t-1} + \sum_{j \in \mathcal{V} \setminus \{i\}} (d_{i,j,o}^t - x_{i,j,o}^t), \quad (4)$$

balancing new arrivals against successful matches. Since autonomous vehicles comply fully with dispatch directives, the idle-vehicle count updates as

$$m_{i,o}^t = m_{i,o}^{t-1} + \sum_{j \in \mathcal{V} \setminus \{i\}} v_{j,i,o}^{\text{arr},t} - \sum_{j \in \mathcal{V} \setminus \{i\}} (x_{i,j,o}^{t-1} + y_{i,j,o}^{t-1}), \quad (5)$$

where $v_{j,i,o}^{\text{arr},t}$ counts vehicles arriving at i from j at time t (completing passenger trips or rebalancing manoeuvres from prior intervals), and the outflow comprises matched departures $x_{i,j,o}^{t-1}$ and rebalancing dispatches $y_{i,j,o}^{t-1}$.

C. Model Architecture

At a high level, the objective for each operator is to learn a policy $\pi(a_t | s_t)$ that maximizes their expected cumulative reward through interactions with the MDP. In our setup, each operator o maintains an independent actor $\pi_{\theta_o}(\cdot | s_t)$ and critic $V_{\phi_o}(s_t)$ with no parameter sharing between operators. The networks take the state s_t (Section III-B) as input and employ a convolutional neural network (GCN) encodings [3], [7] followed by fully connected layers (see appendix). The critic aggregates node embeddings via global summation to produce a scalar value $V_{\phi_o}(s_t)$. The actor outputs strictly positive parameters (via Softplus) that define the stochastic policy. For joint pricing and rebalancing, each region i yields parameters α_i^t and β_i^t for a Beta distribution from which the origin-based price scalar is sampled: $p_{i,o}^t \sim \text{Beta}(\alpha_i, \beta_i)$, and a concentration scalar γ_i^t that collectively form $\gamma^t \in \mathbb{R}^{N_v}$, parameterizing a Dirichlet distribution from which the desired idle-vehicle shares are sampled: $\mathbf{w}_o^t \sim \text{Dirichlet}(\gamma^t)$. For pricing-only or rebalancing-only control, the actor outputs only the Beta or Dirichlet parameters, respectively.

IV. EXPERIMENTS

This section empirically evaluates the proposed framework along two dimensions: (i) performance across San Francisco, Washington DC, and NYC Manhattan South, contrasting monopolistic single-operator control against competitive dual-operator scenarios under rebalancing-only, pricing-only, and joint control modes; and (ii) sensitivity analyses on fleet size, asymmetric fleet distributions, and regional wage heterogeneity and their effects on equilibrium outcomes.

All experiments use a discrete-time simulation environment adapted from [20], spanning the peak evening period (19:00–20:00). Demand is modeled via a Poisson distribution where the rate parameter is derived from real-world taxi trip data [20], [21]. Operators are trained using A2C with the GCN-based architecture described in Section III-C, trained to convergence and evaluated over 10 test runs. We report averages and standard deviations in parentheses.¹

A. Multi-City Performance Analysis

We evaluate performance across three urban environments with distinct characteristics, summarized in Table I. Spatial demand variability is measured by the coefficient of variation (CV), defined as the ratio of the standard deviation to the mean of regional demand. We further report two non-learned benchmark gaps: The no control (“NC”) baseline, corresponding to system performance without rebalancing or pricing interventions, and a uniform distribution heuristic (“UD”), which aims to distribute idle vehicles evenly across the network under fixed prices. The reward gap and served gap measure the relative improvement of equal-distribution over no-control in reward and served passengers, serving as an approximation for the improvement gained by rebalancing.

TABLE I: Scenario characteristics for comparative analysis.

City	Hourly Wage	Nodes	Veh.	Demand	Reward Gap	Served Gap	CV
San Francisco	\$17.76	10	374	5490	46.72%	63.04%	1.31
Washington DC	\$25.26	18	1096	16881	15.14%	48.13%	1.26
NYC Man. South	\$22.77	12	650	21270	10.03%	20.83%	0.69

Note: Veh.: No. Vehicles; CV: Coefficient of Variation of Demand.

1) *Single-Operator Monopolistic Performance:* Tables II and III present total rewards for different control strategies in the single-operator setting. Beyond the no-control and uniform distribution heuristic, learning-based methods include rebalancing-only, pricing-only and a joint policy that controls both decisions simultaneously. The joint policy outperforms all baselines and single-mode policies across all three cities. In San Francisco, joint control achieves a 22.4% improvement over rebalancing alone and a 42.4% improvement over pricing alone. The magnitude of this improvement decreases in cities with lower demand variability: the gain over rebalancing drops to 5.3% in Washington DC, and becomes negligible (0.02%) in NYC Manhattan South. Dynamic pricing, under both pricing-only and joint control policies, leads to a monopolistic increase in prices in both Washington DC and NYC Man South, decreasing the number of served passengers compared to rebalancing with fixed prices.

2) *Dual-Operator Competitive Performance:* Table IV presents total rewards for the dual-operator setting, where, unlike the single-operator case, no single control mode dominates across all cities. In San Francisco, joint control achieves

¹Supplementary material, code and hyperparameter at https://github.com/emto17ab/dual_agent_r1

TABLE II: Single-operator (monopolistic) profits [\\$]. Best policy in bold. We report averages across 10 test runs and std. dev in parentheses

City	NC	UD	Reb.	Pricing	Joint
San Francisco	6345.49 (251.60)	9470.06 (336.71)	10037.29 (337.03)	8629.30 (193.96)	12286.03 (166.74)
Washington DC	13153.97 (324.58)	15630.03 (388.50)	15976.21 (395.37)	13972.47 (301.58)	16816.04 (287.07)
NYC Man. South	16283.02 (487.67)	18221.62 (260.07)	18499.21 (291.51)	17004.39 (504.23)	18503.52 (324.97)

the highest reward (10,415.\$), while Washington DC favors rebalancing (15,620\$). Notably, the rebalancing-only policy serves as a fixed-price benchmark and is unrealistic in practice, as both operators share identical prices and are not in price competition. In NYC Manhattan South, pricing-only control achieves the highest reward (18,632\$), surpassing both alternative modes. This variation suggests that in high-variability environments, fleet positioning is the primary competitive lever, whereas in stable, high-density settings, pricing can effectively function as a mechanism for implicit rebalancing. Furthermore, the inferior performance of the joint policy in NYC South highlights the higher complexity of the joint control problem in the competitive setting, where rebalancing as a long-horizon decision, needs to account for the uncertainty of future demand, that is heavily influenced by the unobserved strategy of the competitor.

TABLE IV: Dual-operator combined profits [\\$]. Best policy in bold.

City	NC	UD	Reb.	Pricing	Joint
San Francisco	6391.2 (232.4)	9352.6 (258.9)	10065.9 (248.7)	8919.0 (160.4)	10415.1 (178.8)
Washington DC	13172.3 (344.6)	15113.5 (325.8)	15619.5 (325.7)	12820.8 (318.2)	13460.6 (247.6)
NYC Man. South	16048.4 (416.6)	17652.0 (277.5)	18133.7 (330.8)	18631.6 (376.7)	17481.1 (258.7)

Table V provides detailed metrics for the dual-operator setting. Several patterns are worth highlighting. First, competition drives prices downward relative to the monopolistic case. Second, waiting times generally increase in the dual-operator setting, reflecting the inefficiency of fragmented fleet management. Third, profit splits between operators are approximately balanced, with typical differences under 2%.

3) *Monopolistic vs. Competitive Comparison*: Comparing the best-performing policies across market structures reveals profit losses induced by competition. In San Francisco, the monopolistic joint control achieves 12,286\$ while the best dual-operator configuration yields 10,415\$, a 15.2% reduction. Washington DC shows a 7.1% reduction. In NYC Manhattan South, the dual-operator pricing strategy achieves a profit, slightly above the monopolistic joint control. This may reflect the effect that competitive pricing stimulates additional demand in this high-density environment, though the difference (0.7%) is neglectable. Generally, pricing competition drives down the prices compared to the monopolistic setting in all

scenarios with up to 27% in San Francisco. The magnitude of competition-induced profit losses appears related to demand variability. High-CV environments suffer larger losses under competition, as fragmented fleet management amplifies the difficulty of matching supply to volatile demand. In the low-CV NYC scenario, the primary competitive dimension shifts from rebalancing efficiency to price-based market share competition, where fragmentation is less costly.

B. Competitive Policy Analysis in NYC Manhattan South

Results in Table IV do not directly reveal any specific pricing behavior, as neither operator consistently, strongly undercuts the other on average. However, a granular analysis of the pricing-only policy in NYC-South reveals that operators have learned to employ strategic, slight undercutting in specific areas to capture demand while avoiding ineffective profit losses from excessive undercuts. This is shown in Figure 6. At $t = 0$, Operator 1 selectively undercuts Operator 0 in four high-demand regions, while Operator 0 undercuts in the remaining zones. The strategies are further marked by a strong regional variance of up to a 83% difference in price scalars between the high-demand regions in the north to low-demand regions in the south. Regarding rebalancing strategies, Figure 2 illustrates that rebalancing patterns of both operators closely track demand patterns, with Operator 0 being more targeted in their rebalancing, and Operator 1 choosing a more balanced strategy.

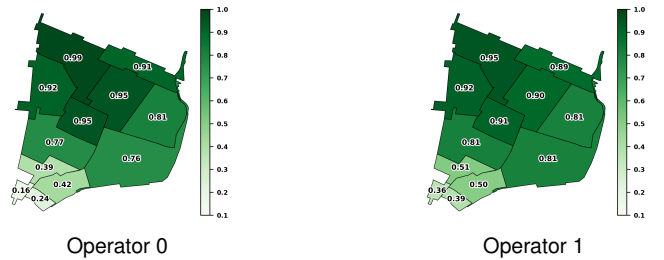


Fig. 1: Initial pricing scalars at timestep 0 for the pricing-only policy in NYC Man. South.

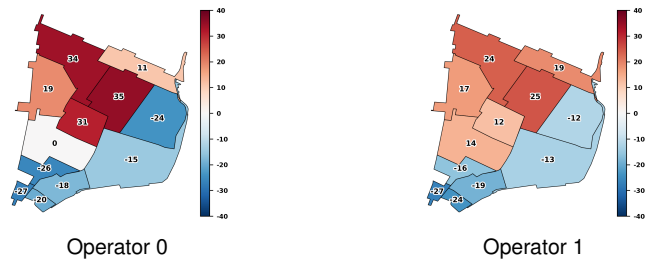


Fig. 2: Net rebalancing flows for the joint control policy, showing cumulative vehicle movements across all time steps. Red = net receiver, blue = net sender.

C. Impact of Pricing Information

We compare scenarios where operators can versus cannot observe competitor prices. Our experiments show that system

TABLE III: Single-operator (monopolistic) performance. “Wait time” corresponds to passenger wait time. Best results are in bold.

Policy	San Francisco			Washington DC			NYC Man. South		
	Reb.	Pricing	Joint	Reb.	Pricing	Joint	Reb.	Pricing	Joint
Reward [\$]	10037.29 (337.03)	8629.30 (193.96)	12286.03 (166.74)	15976.21 (395.37)	13972.47 (301.58)	16816.04 (287.07)	18499.21 (291.51)	17004.39 (504.23)	18503.52 (324.97)
Rebalancing Costs [\$]	877.08 (25.30)	—	650.04 (17.36)	3475.65 (152.04)	—	2975.85 (83.57)	1436.70 (85.48)	—	1712.25 (101.98)
Rebalance Trips	523.70 (12.59)	—	384.00 (13.70)	1085.80 (34.25)	—	955.50 (25.45)	295.90 (20.40)	—	361.10 (23.56)
Price Scalar	—	0.75 (0.00)	0.88 (0.00)	—	1.20 (0.00)	1.02 (0.00)	—	1.07 (0.00)	1.02 (0.00)
Wait time [min.]	0.85 (0.14)	1.49 (0.08)	1.57 (0.15)	1.03 (0.09)	1.25 (0.15)	0.64 (0.09)	1.91 (0.06)	1.48 (0.08)	1.71 (0.10)
Queue	2.03 (0.34)	4.44 (0.26)	5.40 (0.41)	5.56 (0.44)	4.51 (0.42)	3.03 (0.39)	14.20 (0.48)	9.09 (0.40)	12.07 (0.65)
Served Demand	960.90 (30.48)	816.60 (15.14)	1273.70 (16.36)	4182.40 (59.60)	2309.50 (49.93)	3860.30 (44.29)	3571.10 (36.75)	2777.80 (78.12)	3528.10 (39.21)
Total Demand	1092.10 (42.86)	1298.90 (37.03)	1685.60 (35.72)	4753.00 (76.79)	2975.40 (43.52)	4129.40 (54.38)	4705.70 (73.36)	3590.10 (73.90)	4420.00 (77.77)

TABLE V: Dual-operator performance metrics. Best-performing policies are in bold.

Policy	San Francisco			Washington DC			NYC Man. South		
	Reb.	Pricing	Joint	Reb.	Pricing	Joint	Reb.	Pricing	Joint
Total Reward [\$]	10065.9 (248.7)	8919.0 (160.4)	10415.1 (178.8)	15619.5 (325.7)	12820.8 (318.2)	13460.6 (247.6)	18133.7 (330.8)	18631.6 (376.7)	17481.1 (258.7)
Reward Operator 0	5071.5 (178.5)	4191.5 (77.1)	5190.7 (116.7)	7795.7 (233.7)	6386.6 (189.6)	6726.0 (135.8)	9010.8 (242.6)	9351.6 (161.4)	8717.0 (249.1)
Reward Operator 1	4994.4 (159.8)	4727.6 (149.5)	5224.4 (126.3)	7823.8 (117.2)	6434.2 (255.9)	6734.6 (171.4)	9123.0 (341.4)	9280.1 (265.1)	8764.1 (223.5)
Total Reb. Costs [\$]	1006.8 (24.0)	—	549.1 (20.7)	4120.8 (120.2)	—	3368.1 (125.2)	1600.2 (95.4)	—	1379.0 (83.7)
Reb. Costs Operator 0	498.5 (19.3)	—	296.7 (10.6)	2094.8 (88.5)	—	1682.7 (72.1)	813.5 (73.6)	—	699.6 (76.7)
Reb. Costs Operator 1	508.3 (19.0)	—	252.4 (13.3)	2026.0 (59.2)	—	1685.4 (83.3)	786.8 (107.0)	—	679.4 (63.1)
Total Reb. Trips	593.8 (14.4)	—	323.8 (13.5)	1221.9 (47.4)	—	911.1 (37.2)	338.4 (21.2)	—	284.7 (19.0)
Reb. Trips Operator 0	294.0 (11.0)	—	172.3 (5.3)	618.2 (37.0)	—	457.2 (20.4)	173.5 (18.2)	—	144.9 (17.8)
Reb. Trips Operator 1	299.8 (9.7)	—	151.5 (9.8)	603.7 (15.3)	—	453.9 (21.6)	164.9 (24.2)	—	139.8 (14.3)
Total Served Demand	972.3 (23.4)	865.8 (14.4)	1378.9 (17.1)	4239.5 (46.8)	2892.8 (67.6)	4414.4 (33.0)	3535.8 (39.4)	3337.6 (52.3)	3561.1 (29.0)
Served Demand	488.4 (16.1)	403.6 (6.7)	694.5 (12.3)	2124.2 (34.5)	1447.5 (43.7)	2205.9 (18.5)	1758.1 (29.4)	1674.3 (19.1)	1773.9 (26.1)
Served Demand	483.9 (15.1)	462.2 (13.8)	684.4 (11.7)	2115.3 (16.7)	1445.3 (56.6)	2208.5 (21.4)	1777.7 (39.5)	1663.3 (38.7)	1787.2 (24.0)
Price Scalar Operator 0	—	0.72 (0.00)	0.64 (0.00)	—	0.97 (0.00)	0.90 (0.00)	—	0.95 (0.00)	0.96 (0.00)
Price Scalar Operator 1	—	0.72 (0.00)	0.67 (0.00)	—	0.98 (0.00)	0.90 (0.00)	—	0.95 (0.01)	0.96 (0.00)
Wait time Operator 0 [min]	0.84 (0.18)	1.57 (0.07)	1.95 (0.11)	0.88 (0.06)	1.73 (0.07)	1.73 (0.17)	1.80 (0.08)	1.51 (0.08)	2.03 (0.10)
Wait time Operator 1 [min]	0.86 (0.17)	1.68 (0.12)	1.85 (0.11)	0.87 (0.12)	1.77 (0.06)	1.71 (0.12)	1.78 (0.07)	1.45 (0.08)	2.06 (0.08)
Queue Operator 0	2.24 (0.65)	3.44 (0.84)	5.29 (0.82)	1.98 (0.85)	6.11 (0.57)	5.84 (0.89)	8.41 (1.12)	5.69 (0.73)	10.4 (1.3)
Queue Operator 1	2.71 (0.63)	3.87 (0.52)	3.23 (0.66)	2.04 (0.73)	5.89 (0.83)	5.53 (1.25)	7.75 (1.05)	4.96 (0.67)	10.8 (1.2)
Total Demand	1112.5 (43.3)	1519.5 (34.2)	2154.1 (40.9)	4746.9 (76.8)	4990.6 (73.0)	5682.0 (92.1)	4683.0 (73.9)	4311.7 (65.1)	5231.3 (61.6)
Demand Operator 0	551.9 (20.2)	721.3 (25.2)	1192.4 (32.5)	2379.4 (54.5)	2544.8 (49.7)	2859.9 (51.2)	2336.2 (56.0)	2145.4 (36.7)	2581.1 (59.5)
Demand Operator 1	560.6 (30.9)	798.2 (14.5)	961.7 (21.3)	2367.5 (36.6)	2445.8 (29.0)	2822.1 (44.0)	2346.8 (39.4)	2166.3 (34.7)	2650.2 (42.1)

performance is robust to this information condition across all policy modes, with converged rewards nearly identical, suggesting competitor prices may introduce noise rather than actionable signal in the scenarios of simultaneous learning from scratch. Full training curves in appendix.

D. Fleet Size Sensitivity Analysis

We compare system performance under varying fleet sizes (evenly split between operators) for the joint policy, no control, and uniform distribution baselines in NYC Man. South. The joint policy dynamically lowers price scalars as fleet size grows (from 1.04 to 0.71) to maintain utilization of the larger fleet, serving up to 64% more passengers than NC. Total reward peaks at 1,050 vehicles and declines beyond this point as rebalancing costs outpace revenue gains, suggesting dimin-

ishing profit from fleet expansion. Full results are available appendix.

E. Fleet Split Sensitivity Analysis

We evaluate the joint policy in NYC Man. South under five asymmetric fleet splits ranging from 5:5 to 1:9 between the two operators. Total reward is highest at the 4:6 split (17,567 \$) and degrades at more extreme asymmetries, while total served demand remains stable across configurations (3,500-3,577). The smaller operator compensates for its limited capacity by raising prices (from 0.96 at 5:5 to 1.10 at 1:9), whereas the larger fleet of the other operator allows to consistently undercut (0.93-0.96). These results indicate, that fleet size imbalances reduces direct price competition. Full results are available in appendix.

F. Regional Wage Heterogeneity

Lastly, we evaluate the impact of spatially varying passenger incomes by conducting experiments in NYC Manhattan South, where regional wages range from \$10 to \$30, with a total fleet of 650 vehicles evenly split between operators. Notably, rebalancing flows reveal spatial adaptation, with both operators repositioning vehicles from low-income regions toward high-income areas where demand is concentrated, while pricing scalars are increased to exploit higher willingness to pay- full results are provided in appendix.

V. SUMMARY AND CONCLUSION

This paper introduced a competitive multi-operator reinforcement learning framework for joint pricing and fleet rebalancing in AMoD systems to study how competition impacts operator policy learning. By embedding a discrete choice model within the learning loop, passenger allocation emerges endogenously through utility maximization, coupling pricing actions to demand competition. Crucially, we empirically show that learning-based approaches remain robust to the additional stochasticity introduced by competition. Competitive agents converge to stable rewards and learn policies that effectively rebalance fleets and set dynamic prices while accounting for unobserved competitor behavior.

Experiments across three cities yield several key findings. Under monopoly, joint pricing and rebalancing consistently maximizes profit. Competition fundamentally alters which strategies dominate: while joint control excels under monopoly, competitive markets can favor specialized policies.

Competition drives prices down, benefiting passengers through lower fares, but multi-operator fleet management increases waiting times, illustrating mixed welfare effects. Sensitivity analyses show that operators dynamically adapt to fleet size changes, asymmetric fleet splits reduces direct pricing competition where smaller operators raise prices while larger ones undercut, and wage heterogeneity drives fleet repositioning toward high-income areas and increase the prices to exploit higher willingness to pay.

These findings suggest several directions for future work: incorporating granular waiting time beyond a maximum threshold into passenger utilities to introduce a direct trade-off between profitability and service quality, investigating emergent behaviors induced by asymmetric architectures or learning parameters, and explicitly modeling collusive behavior to analyze its impact on pricing and consumer welfare.

REFERENCES

- [1] A. A. Ceder, "Urban mobility and public transport: future perspectives and review," *Int. J. Urban Sci.*, vol. 25, no. 4, pp. 455–479, 2021.
- [2] Z. Wang and S. Li, "Competition between autonomous and traditional ride-hailing platforms: Market equilibrium and technology transfer," *Transp. Res. Part C: Emerg. Technol.*, vol. 165, p. 104728, 2024.
- [3] D. Gammelli, K. Yang, J. Harrison, F. Rodrigues, F. C. Pereira, and M. Pavone, "Graph neural network reinforcement learning for autonomous mobility-on-demand systems," in *IEEE Conf. on Decision and Control (CDC)*, 2021, pp. 2996–3003.

- [4] J. Wen, J. Zhao, and P. Jaillet, "Rebalancing shared mobility-on-demand systems: A reinforcement learning approach," in *IEEE Int. Conf. on Intell. Transp. Syst. (ITSC)*, 2017, pp. 220–225.
- [5] Z. Lei and S. V. Ukkusuri, "Scalable reinforcement learning approaches for dynamic pricing in ride-hailing systems," *Transp. Res. Part B: Methodol.*, vol. 178, p. 102848, 2023.
- [6] C. Chen, F. Yao, D. Mo, J. Zhu, and X. M. Chen, "Spatial-temporal pricing for ride-sourcing platform with reinforcement learning," *Transp. Res. Part C: Emerg. Technol.*, vol. 130, p. 103272, 2021.
- [7] X. Li, C. Schmidt, D. Gammelli, and F. Rodrigues, "Learning joint rebalancing and dynamic pricing policies for autonomous mobility-on-demand," *IEEE Trans. Intell. Transp. Syst.*, vol. 26, no. 10, pp. 16619–16634, 2025.
- [8] R. Zhang and M. Pavone, "Control of robotic mobility-on-demand systems: A queueing-theoretical perspective," *Int. J. Robot. Res.*, vol. 35, no. 1-3, pp. 186–203, 2016.
- [9] G. C. Calafiore, C. Bongiorno, and A. Rizzo, "A robust mpc approach for the rebalancing of mobility on demand systems," *Control Eng. Pract.*, vol. 90, pp. 169–181, 2019.
- [10] X. Guo, N. S. Caros, and J. Zhao, "Robust matching-integrated vehicle rebalancing in ride-hailing system with uncertain demand," *Transp. Res. Part B: Methodol.*, vol. 150, pp. 161–189, 2021.
- [11] R. Iglesias, F. Rossi, K. Wang, D. Hallac, J. Leskovec, and M. Pavone, "Data-driven model predictive control of autonomous mobility-on-demand systems," in *IEEE Int. Conf. on Robot. and Autom. (ICRA)*, 2018, pp. 6019–6025.
- [12] L. Tresca, C. Schmidt, J. Harrison, F. Rodrigues, G. Zardini, D. Gammelli, and M. Pavone, "Robo-taxi fleet coordination at scale via reinforcement learning," 2025, arXiv:2504.06125.
- [13] G. P. Cachon, K. M. Daniels, and R. Lobel, "The role of surge pricing on a service platform with self-scheduling capacity," *Operations Strategy eJournal*, 2016.
- [14] Y. Guan, "Design and optimization of shared mobility on demand: Dynamic routing and dynamic pricing," Ph.D. dissertation, Massachusetts Institute of Technology, 2021.
- [15] W. Tang, H. Wang, Y. Wang, C. Chen, and X. Chen, "A bi-level optimization model for ride-sourcing platform's spatial pricing strategy," *J. Adv. Transp.*, vol. 2022, pp. 1–22, 2022.
- [16] Y. Yang and M. Ramezani, "The intraday competition in a duopoly ride-hailing market," in *12th Triennial Symp. on Transp Analysis*, 2025.
- [17] R. Engelhardt, P. Malcolm, F. Dandl, and K. Bogenberger, "Competition and cooperation of autonomous ridepooling services: Game-based simulation of a broker concept," *Front. Future Transp.*, vol. 3, 2022.
- [18] G. Zardini, N. Lanzetti, G. Belgioioso, C. Hartnik, S. Bolognani, F. Dörfler, and E. Frazzoli, "Strategic interactions in multi-modal mobility systems: A game-theoretic perspective," in *IEEE Int. Conf. on Intell. Transp. Syst. (ITSC)*, 2023, pp. 5452–5459.
- [19] D. Khulbe, R. Seshadri, and M. Ben-Akiva, "A probabilistic simulation framework to assess the impacts of ridesharing and congestion charging in new york city," *Data Sci. Transp.*, vol. 5, no. 1, pp. 1–25, 2023.
- [20] D. Gammelli, K. Yang, J. Harrison, F. Rodrigues, F. Pereira, and M. Pavone, "Graph meta-reinforcement learning for transferable autonomous mobility-on-demand," in *Proc. ACM SIGKDD Conf. on Knowl. Discovery and Data Mining*, 2022, pp. 2913–2923.
- [21] B. Donovan and D. Work, "New york city taxi trip data (2010-2013)," 2016, univ. of Illinois Urbana-Champaign.
- [22] U.S. Census Bureau, "Income in the past 12 months (table s1901), american community survey," 2013, data.census.gov, Acc. 2026-01-13.

APPENDIX

VEHICLE REBALANCING MODEL

At each time step t , the model determines the rebalancing flows $\{y_{i,j,o}^t\}$ for operator o that minimize the total rebalancing cost while satisfying the desired vehicle distribution specified by the actor network. The optimization problem is formulated as:

$$\min \sum_{(i,j) \in \mathcal{E}} c_{i,j,o}^t y_{i,j,o}^t \quad (6)$$

$$\text{s.t.} \sum_{j \neq i} (y_{j,i,o}^t - y_{i,j,o}^t) + m_{i,o}^t \geq \tilde{m}_{i,o}^t, \quad i \in \mathcal{V} \quad (7)$$

$$\sum_{j \neq i} y_{i,j,o}^t \leq m_{i,o}^t, \quad i \in \mathcal{V} \quad (8)$$

$$y_{i,j,o}^t \geq 0, \quad (i,j) \in \mathcal{E} \quad (9)$$

where $\tilde{m}_{i,o}^t$ denotes the number of desired vehicles at region i for operator o at time t . Objective (6) minimizes the rebalancing cost. Constraint (7) ensures that the desired vehicle number is satisfied, accounting for the current idle vehicles $m_{i,o}^t$ and the net inflow of rebalanced vehicles. Constraint (8) limits the rebalancing flow from each region by the number of available idle vehicles. The desired vehicle distribution is calculated by $\tilde{m}_{i,o}^t = \lfloor w_{i,o}^t \sum_{i \in \mathcal{V}} m_{i,o}^t \rfloor$, where $w_{i,o}^t$ is the rebalancing weight output by the actor network for region i . Note that the constraint matrix of this network flow problem is totally unimodular, and since both $m_{i,o}^t$ and $\tilde{m}_{i,o}^t$ are integer-valued, the optimal solution is guaranteed to be integral.

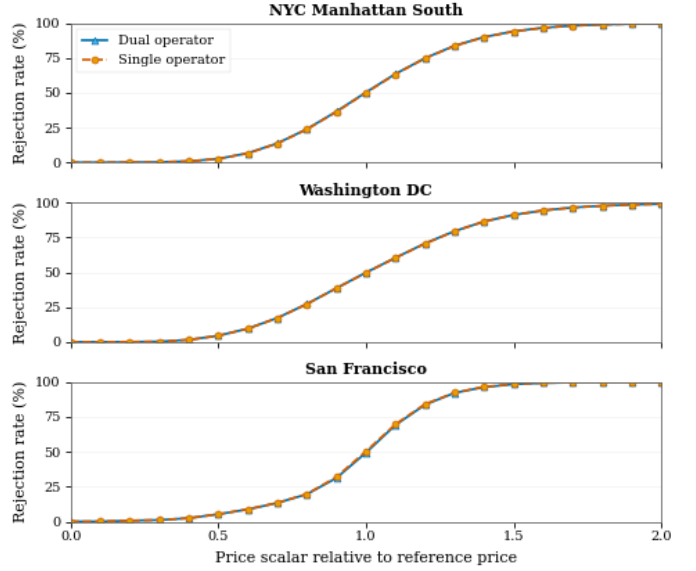


Fig. 3: Rejection rate versus price scalar relative to the historical reference price across studied datasets for both single and dual-operator setups, with the model calibrated to a 50% rejection rate at the historical reference price.

PARAMETERS USED IN TRAINING

Category	Hyperparameter	Value
Training	Actor learning rate (α_π)	2×10^{-4}
	Critic learning rate (α_V)	4×10^{-4}
	Discount factor (γ)	0.97
	Reward scaling factor	4,000
	Actor gradient clip	1,000
	Critic gradient clip	1,000
	Critic warmup episodes	50
	Training episodes	150,000
Network	Hidden layer size	256
	Look-ahead horizon (T)	6
	Scale factor	0.01
Price Scalars	Observe OD-prices	Yes
	OD-price scalars	No

THREE-STEP CONTROL ARCHITECTURE

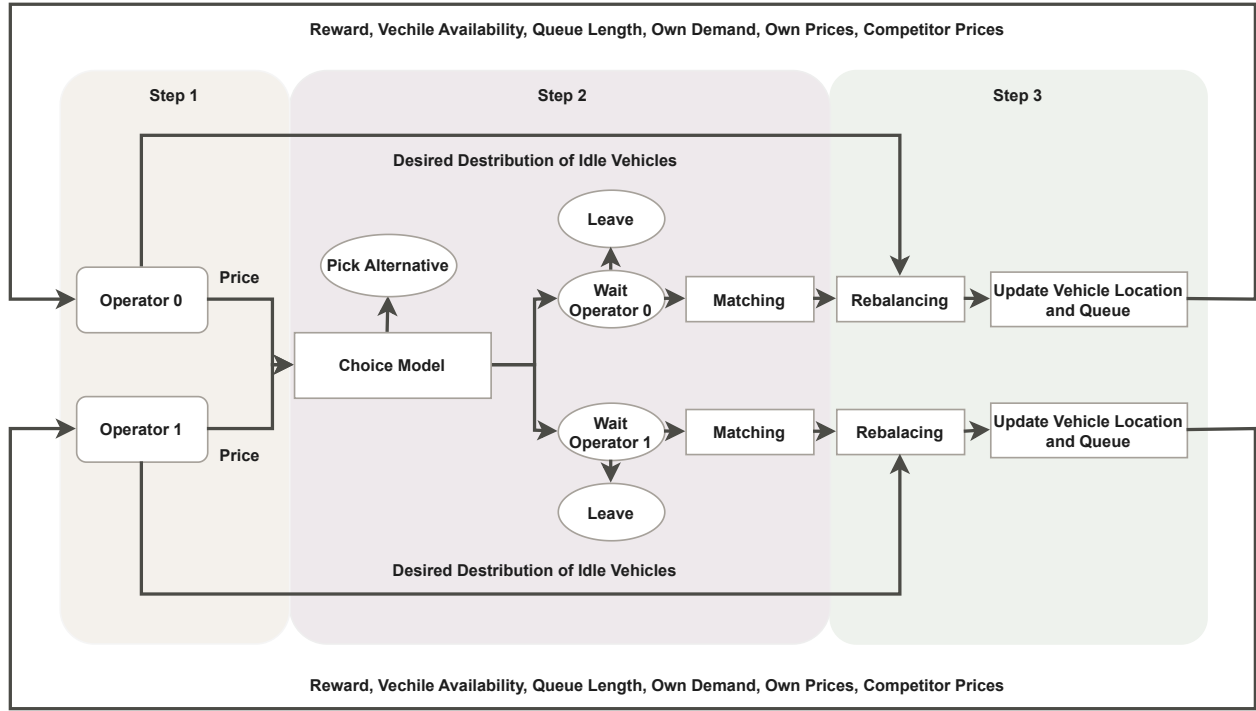


Fig. 4: Three-step control architecture for dual-operator AMoD control. Step 1: operators formulate pricing and desired idle-vehicle distribution policies. Step 2: passenger assignment via choice model, queuing, and matching. Step 3: idle-vehicle rebalancing and update of vehicle positions and queues.

OPERATOR ARCHITECTURE

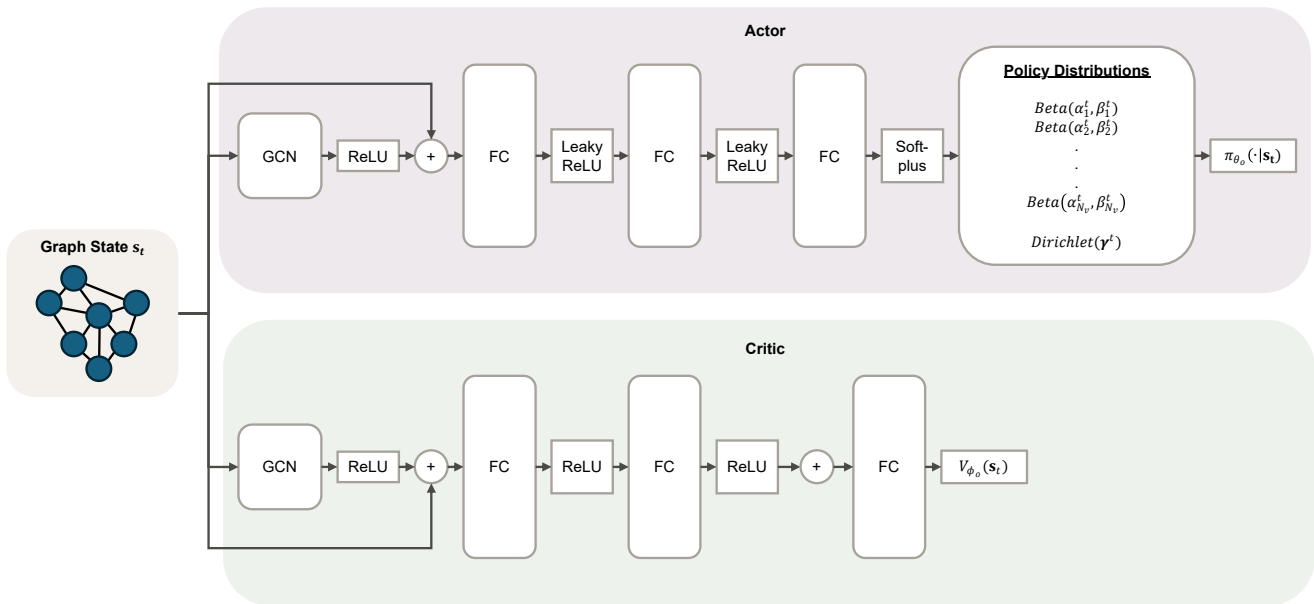


Fig. 5: The Actor-Critic architecture employed by the operators. Each operator maintains independent actor and critic networks.

PRICING SCALARS UNDER PRICING-ONLY POLICY NYC

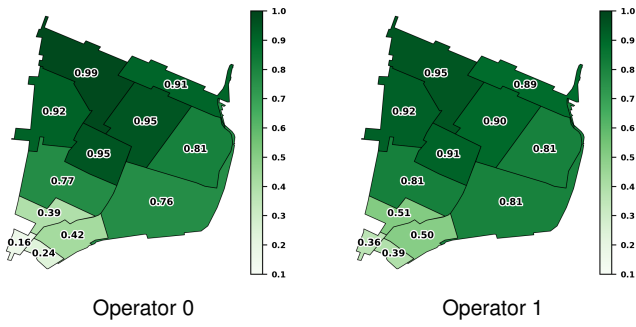


Fig. 6: Initial pricing policies at timestep 0 for the pricing-only policy.

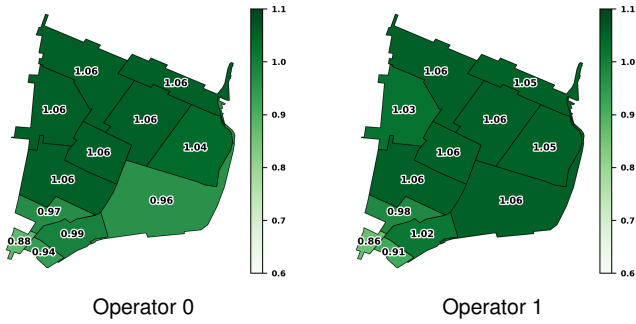


Fig. 7: Final pricing policies at time step 19 for the pricing-only policy.

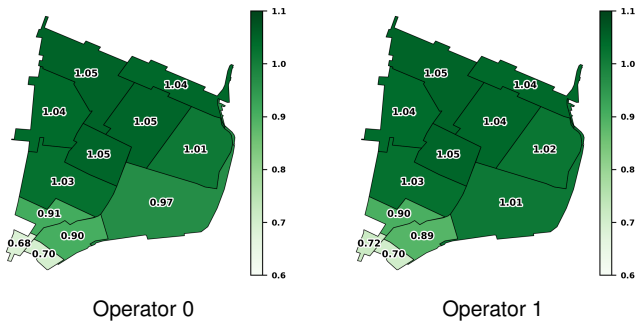


Fig. 8: Time-averaged pricing scalars for the pricing-only policy, computed across all 20 time steps.

FLEET SIZE SENSITIVITY

Fleet Size	Joint Policy						NC			UD				
	Reward	Served	Rebal. Costs	Rebal. Trips	Price A0	Price A1	Reward	Served	Price Both	Reward	Served	Rebal. Costs	Rebal. Trips	Price Both
450	14170.5 (251.7)	2563.9 (28.4)	865.6 (66.9)	177.3 (16.0)	1.04 (0.00)	1.04 (0.00)	12270.7 (251.8)	2550.6 (15.9)	1.00 (0.00)	13217.4 (153.7)	2550.6 (15.9)	989.0 (70.0)	200.6 (16.6)	1.00 (0.00)
650	17481.1 (258.7)	3561.1 (29.0)	1379.0 (83.7)	284.7 (19.0)	0.96 (0.00)	0.96 (0.00)	16048.4 (416.6)	2894.2 (73.9)	1.00 (0.00)	17652.0 (277.5)	3496.5 (32.2)	1865.1 (98.3)	387.9 (19.6)	1.00 (0.00)
850	19513.1 (288.1)	4538.7 (38.9)	1871.0 (79.9)	386.3 (16.7)	0.88 (0.00)	0.88 (0.00)	18683.9 (461.8)	3367.4 (83.3)	1.00 (0.00)	19941.6 (334.8)	4171.5 (44.7)	3401.8 (128.6)	761.5 (27.2)	1.00 (0.00)
1050	20373.0 (198.7)	5512.9 (30.1)	2152.1 (77.1)	446.8 (19.7)	0.79 (0.00)	0.79 (0.00)	20667.8 (467.6)	3714.9 (83.3)	1.00 (0.00)	20450.0 (543.4)	4538.1 (72.0)	5016.9 (155.3)	1187.7 (41.2)	1.00 (0.00)
1250	20305.6 (235.2)	6440.1 (32.2)	2509.8 (117.9)	526.9 (29.9)	0.71 (0.00)	0.70 (0.00)	21955.0 (397.2)	3934.1 (71.2)	1.00 (0.00)	19798.1 (526.1)	4639.2 (77.2)	6259.8 (192.8)	1501.7 (46.1)	1.00 (0.00)

FLEET SPLIT SENSITIVITY

Fleet Split (O0:O1)	Total Reward	O0 Reward	O1 Reward	Total Rebal. Trips	O0 Rebal. Trips	O1 Rebal. Trips	O0 Price	O1 Price	Total Served	O0 Served	O1 Served
5:5	17481.1 (258.7)	8717.0 (249.1)	8764.1 (223.5)	284.7 (19.0)	144.9 (17.8)	139.8 (14.3)	0.96 (0.00)	0.96 (0.00)	3561.1 (29.0)	1773.9 (26.1)	1787.2 (24.0)
4:6	17567.0 (231.0)	7295.2 (136.2)	10271.7 (243.7)	279.2 (17.8)	116.1 (12.6)	163.1 (14.6)	0.98 (0.00)	0.95 (0.00)	3577.2 (27.9)	1437.2 (14.7)	2140.0 (30.1)
3:7	17434.2 (241.7)	5772.6 (143.7)	11661.6 (259.2)	285.3 (19.8)	79.6 (11.5)	205.7 (18.9)	1.01 (0.00)	0.94 (0.00)	3562.5 (32.1)	1090.1 (17.4)	2472.4 (33.0)
2:8	16968.2 (263.3)	4140.0 (88.8)	12828.2 (244.2)	294.5 (21.2)	41.3 (4.9)	253.2 (19.8)	1.04 (0.00)	0.93 (0.00)	3530.7 (33.5)	742.3 (13.6)	2788.4 (31.9)
1:9	16655.4 (291.8)	2348.7 (77.9)	14306.7 (299.7)	311.6 (22.3)	14.1 (3.0)	297.5 (22.9)	1.10 (0.00)	0.93 (0.00)	3499.9 (35.8)	380.7 (8.7)	3119.2 (38.1)

IMPACT OF PRICING INFORMATION

Policy	No Information Sharing			Information Sharing		
	Reb.	Pricing	Joint	Reb.	Pricing	Joint
Total Reward	18096.6 (296.6)	18983.6 (267.4)	17689.4 (242.4)	18133.7 (330.8)	18631.6 (376.7)	17481.1 (258.7)
Reward Operator 0	8981.1 (227.9)	9413.0 (111.9)	8951.6 (212.4)	9010.8 (242.6)	9351.6 (161.4)	8717.0 (249.1)
Reward Operator 1	9115.5 (317.0)	9570.6 (192.9)	8737.8 (190.5)	9123.0 (341.4)	9280.1 (265.1)	8764.1 (223.5)
Total Rebalancing Costs	1544.4 (110.7)	—	1349.7 (76.5)	1600.2 (95.4)	—	1379.0 (83.7)
Rebal. Costs Operator 0	806.0 (78.6)	—	662.5 (65.8)	813.5 (73.6)	—	699.6 (76.7)
Rebal. Costs Operator 1	738.5 (103.5)	—	687.1 (59.2)	786.8 (107.0)	—	679.4 (63.1)
Total Rebalance Trips	327.8 (25.4)	—	276.5 (16.8)	338.4 (21.2)	—	284.7 (19.0)
Rebal. Trips Operator 0	172.0 (20.6)	—	134.7 (15.3)	173.5 (18.2)	—	144.9 (17.8)
Rebal. Trips Operator 1	155.8 (23.6)	—	141.8 (12.4)	164.9 (24.2)	—	139.8 (14.3)
Total Served Demand	3521.9 (34.2)	3388.9 (38.1)	3579.5 (29.0)	3535.8 (39.4)	3337.6 (52.3)	3561.1 (29.0)
Served Demand Operator 0	1751.8 (26.1)	1678.1 (13.8)	1800.4 (25.4)	1758.1 (29.4)	1674.3 (19.1)	1773.9 (26.1)
Served Demand Operator 1	1770.1 (36.8)	1710.8 (28.8)	1779.1 (21.0)	1777.7 (39.5)	1663.3 (38.7)	1787.2 (24.0)
Price Operator 0	—	0.96 (0.00)	0.96 (0.00)	—	0.95 (0.00)	0.96 (0.00)
Price Operator 1	—	0.95 (0.01)	0.96 (0.00)	—	0.95 (0.01)	0.96 (0.00)
Wait/mins Operator 0	1.82 (0.08)	1.34 (0.06)	1.97 (0.10)	1.80 (0.08)	1.51 (0.08)	2.03 (0.10)
Wait/mins Operator 1	1.81 (0.07)	1.37 (0.07)	2.06 (0.09)	1.78 (0.07)	1.45 (0.08)	2.06 (0.08)
Queue Operator 0	8.37 (1.09)	4.35 (0.70)	9.89 (1.12)	8.41 (1.12)	5.69 (0.73)	10.4 (1.3)
Queue Operator 1	7.78 (1.21)	4.62 (0.80)	10.7 (1.4)	7.75 (1.05)	4.96 (0.67)	10.8 (1.2)
Total Demand	4683.0 (73.9)	4202.3 (55.2)	5185.7 (58.2)	4683.0 (73.9)	4311.7 (65.1)	5231.3 (61.6)
Demand Operator 0	2336.2 (56.0)	2075.3 (34.3)	2552.0 (52.5)	2336.2 (56.0)	2145.4 (36.7)	2581.1 (59.5)
Demand Operator 1	2346.8 (39.4)	2127.0 (31.8)	2633.7 (34.4)	2346.8 (39.4)	2166.3 (34.7)	2650.2 (42.1)

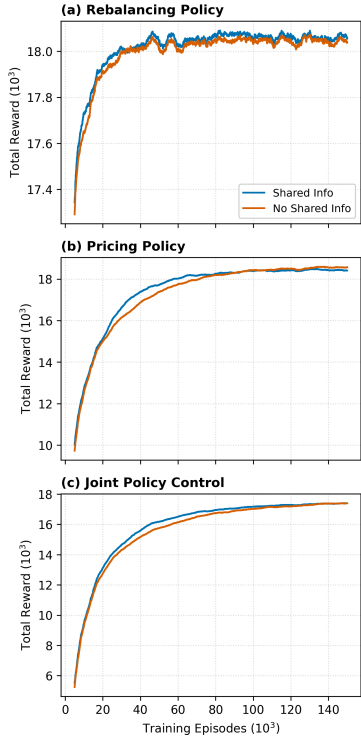


Fig. 9: Convergence dynamics comparing scenarios with and without competitor price visibility: (a) Rebalancing, (b) Pricing, (c) Joint. Curves are smoothed over 30 episodes; the first 5,000 episodes are excluded for clarity. Note that rewards are training rewards based on sampling from the policy distributions and may therefore be lower than test rewards.

REGIONAL WAGE HETEROGENEITY

Metric	Joint Policy
Total Reward	23564.6 (341.1)
Reward Operator 0	11659.3 (206.4)
Reward Operator 1	11905.3 (248.4)
Total Rebalancing Costs	2661.3 (87.2)
Rebalancing Costs Operator 0	1359.8 (52.2)
Rebalancing Costs Operator 1	1301.5 (57.0)
Total Rebalance Trips	609.7 (21.0)
Rebalance Trips Operator 0	315.0 (10.9)
Rebalance Trips Operator 1	294.7 (15.0)
Total Served Demand	2990.9 (28.1)
Served Demand Operator 0	1480.6 (18.9)
Served Demand Operator 1	1510.3 (21.1)
Price Operator 0	1.32 (0.00)
Price Operator 1	1.31 (0.00)
Wait/mins Operator 0	1.42 (0.07)
Wait/mins Operator 1	1.46 (0.09)
Queue Operator 0	6.40 (1.01)
Queue Operator 1	5.97 (1.34)
Total Demand	3567.0 (46.7)
Demand Operator 0	1762.8 (24.5)
Demand Operator 1	1804.2 (33.7)
Average Wage	25.8 (0.1)

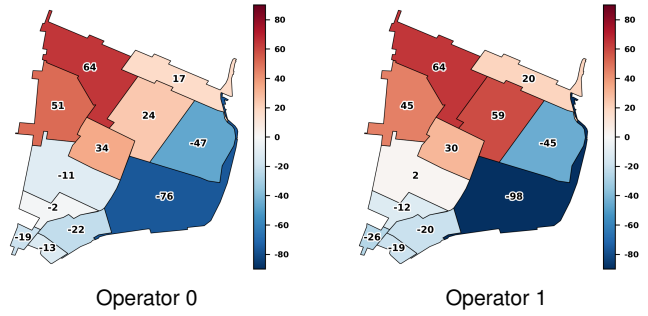


Fig. 11: Net rebalancing flows under regional income heterogeneity, showing cumulative vehicle movements across all time steps. Red = net receiver, blue = net sender.

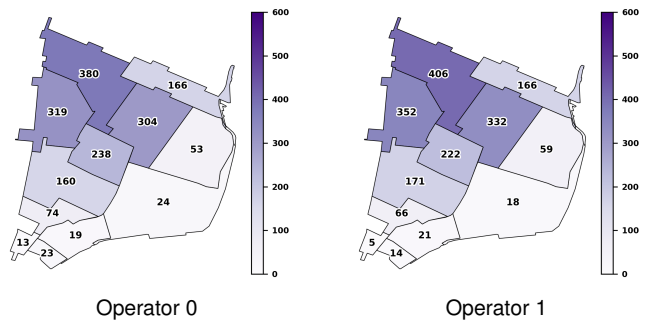


Fig. 12: Total demand originating from each region under regional income heterogeneity.

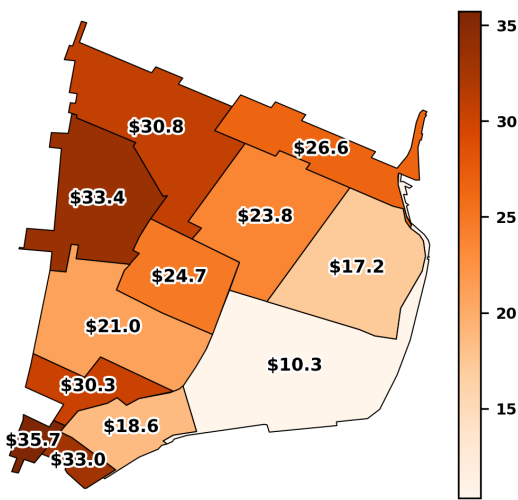


Fig. 10: Average hourly passenger wage distribution across regions in NYC Manhattan South under regional income heterogeneity.

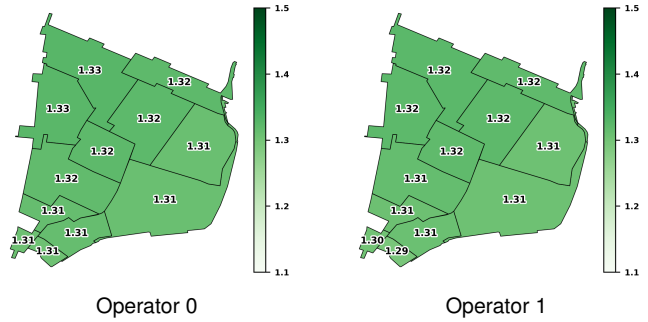


Fig. 13: Average pricing scalars per region across all time steps under regional income heterogeneity.